Click Here for Full Article

Observations of supercooling and frazil ice formation in the Laptev Sea coastal polynya

Igor A. Dmitrenko,[1] Carolyn Wegner,[1] Heidemarie Kassens,[1] Sergey A. Kirillov,[2] Thomas Krumpen,[3] Günther Heinemann,[4] Alfred Helbig,[4] David Schröder,[4] Jens A. Hölemann,[3] Torben Klagge,[1] Konstantin P. Tyshko,[2] and Thomas Busche[5]

[1]   This paper examines a hydrographic response to the wind-driven coastal polynya activity over the southeastern Laptev Sea shelf for April–May 2008, using a combination of Environmental Satellite (Envisat) advanced synthetic aperture radar (ASAR) and TerraSAR-X satellite imagery, aerial photography, meteorological data, and SBE-37 salinity-temperature-depth and acoustic Doppler current profiler land-fast ice edge-moored instruments. When ASAR observed the strongest end-of-April polynya event with frazil ice formation, the moored instruments showed maximal acoustical scattering within the surface mixed layer, and the seawater temperatures were either at or 0.02°C below freezing. We also find evidence of the persistent horizontal temperature and salinity gradients across the fast ice edge to have the signature of geostrophic flow adjustment as predicted by polynya models.

1.   Introduction

[2]   The Siberian continental shelf is known for active water mass transformation in winter due to the seasonal sea-ice formation. In the absence of sensible ocean heat input from below, the offshore components of winter surface wind, forcing over the Siberian coast, create persistent areas of open water off the land-fast ice known as the Great Siberian Polynya [*Bareiss and Görgen*, 2005; *Martin and Cavalieri*, 1989]. As a result, the polynya open water is exposed to the cold air temperature down to −35°C. Under these conditions, the surface water layer supercools. Super-cooled water is water in a liquid state at temperatures below the freezing point in reference to the surface (potentially su-percooled) or the in situ freezing point (in situ supercooled) [*Skogseth et al.*, 2009]. Criteria for formation of in situ supercooled water were suggested by *Coachman* [1966] to be (1) a large net heat loss from the water and (2) transport of the supercooled water away from the existing ice before crys-tallization can take place. Supercooling results in ice forma-tion that occurs initially throughout the surface water layer in the form of small millimeter-scale crystals, called frazil ice crystals, that float slowly to the surface. The frazil ice for-mation results in strong salt input to the underlying shelf water because of brine release. From these considerations, supercooling might play a critical role in the shelf salt budget and sea-ice production [*Drucker et al.*, 2003]. While frazil ice formation in the Arctic was carefully examined over the past several years for the St. Lawrence Island and the Storfjord polynyas [*Danielson et al.*, 2006; *Drucker et al.*, 2003; *Skogseth et al.*, 2008, 2009], the processes controlling the sea-ice growth due to supercooled water and frazil ice for-mation over the Siberian Arctic shelf remain poorly under-stood, owing to the scarce instrumental records and extreme climatic conditions.

[3]   During summer the Siberian shelf hydrography is mainly forced by Siberian river runoff and seasonal sea-ice melting, resulting in substantial surface layer freshening. For example, over the southeastern Laptev Sea, the summer mean surface layer salinity is ~5–15 psu (I. A. Dmitrenko et al., Summer river runoff preconditions the Laptev Sea coastal polynya hydrography: Evidence from summer-to-winter hydrographic records of 2007–2009, submitted to *Continental Shelf Research*, 2010). In contrast, winter ther-modynamic ice formation (accompanied by a very limited inflow of river water) provides salt input to the surface layer through brine release, resulting in a summer-to-winter sur-face salinity difference (~5 psu for the southeastern Laptev Sea; Dmitrenko et al., submitted manuscript, 2010).

[4]   The coastal polynya area is most efficient in providing salt input to the underlying shelf water. Over the Siberian coast, polynyas are most distinct in the Laptev Sea [*Zakharov*,

[1]Leibniz Institute of Marine Sciences at University of Kiel (IFM-GEOMAR), Kiel, Germany.
[2]Arctic and Antarctic Research Institute, St. Petersburg, Russia.
[3]Alfred Wegener Institute for Polar and Marine Research, Bremerhaven, Germany.
[4]Department of Environmental Meteorology, University of Trier, Trier, Germany.
[5]German Aerospace Center, Microwaves and Radar Institute, Oberpfaffenhofen-Wessling, Germany.
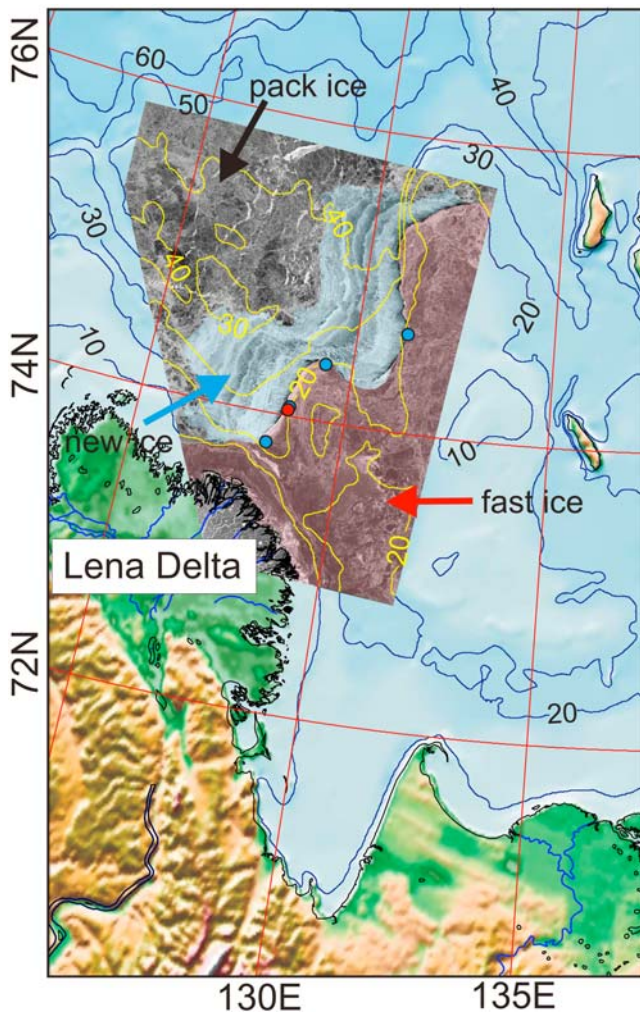
Figure 1. The region of the West New Siberian (WNS) coastal polynya with overlaid Envisat advanced synthetic aperture radar (ASAR) image from 1 May 2008. The light shaded strips emphasized by blue shading are associated with newly formed 5–30 cm thick columnar sea-ice. The fast ice edge separates the land-fast ice to the southeast (emphasized by pink shading) from the newly formed ice and pack ice (gray area) to the northwest. Some ambiguity in the interpretation of newly formed sea-ice and surrounding older fractions may occur. Blue and red dots mark moorings deployed along the land-fast ice edge. Blue dots identify positions of the automated weather stations (AWS). Bathymetry is shown by blue and yellow solid lines.

1997]. As a part of the Russian-German project framework "Laptev Sea System," a fieldwork program was conducted in the West New Siberian (WNS) coastal polynya of the Laptev Sea in April 2008 to study the shelf hydrography response to polynya activity. Our purpose here is to examine the local oceanographic effects of the wind-forced polynya over the shallow shelf with a focus on supercooled water and determination of frazil ice formation. Our examination is based on both satellite imagery and measurements from moored instruments recording between April and May 2008 in the

vicinity of the Lena Delta in the southeastern Laptev Sea (Figure 1).

2. Data and Methods

[5] Between April and May 2008, five moorings were deployed from the stationary land-fast ice 10–800 m apart in the fast ice edge contouring the onshore perimeter of the WNS coastal polynya (Figure 1). The paper focuses on the results at mooring site M2 (for position, see Figure 2), which was deployed beneath 57 cm thick land-fast ice 10 m from the fast-ice edge; by the time of recovery, the M2 was situated beneath 87 cm thick fast ice, ~1 km from the fast ice edge. All moorings carried a combination of 300 kHz downward-looking Workhorse Sentinel acoustic Doppler current profilers (ADCPs) by Teledyne RD Instruments, and Sea-Bird Electronics, Inc., SBE-37s (unpumped) with conductivity-temperature-depth (CTD) sensors. The SBE-37s provided a 1 min interval for sampling conductivity, temperature, and pressure at fixed depths in the surface (~4.5 m) and bottom (~17.5 m) water layers. The velocity and acoustic backscatter intensity data from the ADCPs were taken at 1 m depth intervals, with a 5 min ensemble time interval and 60 pings per ensemble. The first bin was located at ~5.4 m. All moorings were anchored at ~20 m water depth (Figure 1). Mooring-based observations were complemented by episodic CTD profiling at the mooring positions taken with an SBE-19+ CTD.

[6] According to the manufacturers' estimates, individual temperature and conductivity measurements are accurate to ±0.005°C and ±0.0005 S/m, respectively, for the SBE-19+, and to ±0.002°C and ±0.0003 S/m, respectively, for the SBE-37s. The ADCP velocity precision and resolution are ±0.5% and ±0.1 cm/s, respectively. The ADCP velocity estimated error was 1.8 cm/s. Compass accuracy is ±2.7°. The current direction was corrected by adding mean magnetic deviation (−16°). The precision of the ADCP echo intensity data is ±1.5 dB. The CTDs were calibrated before the expedition. Frazil crystals smaller than ~100 μm could cause a permanent reduction in conductivity cell of SBE-37s [*Skogseth et al.*, 2009]. In contrast, our SBE-37 record from M2 looks rather reliable, having no rapid spikes in salinity-conductivity raw data that could be attributed to the frazil ice crystals inside the conductivity cell.

[7] To monitor the WNS coastal polynya as a whole, 26 Environmental Satellite (Envisat) advanced synthetic aperture radar (SAR) and 10 TerraSAR-X images were acquired between April and May 2008. SAR satellite-mounted instruments transmit radar signals and then measure how strongly those signals are scattered back. In general, the newly formed sea-ice, polynya open water, frazil ice, and land-fast ice edge all exhibit substantially different scattering signatures and are therefore distinguishable on radar imagery. Darker areas in the image (Figures 1, 2, 3a, and 3b) represent low backscatter, whereas lighter areas represent high backscatter. Lighter features indicate rough surfaces (newly formed sea-ice, rough water surface with frazil ice, ice-ridged surface) that return radar signals of various strengths, all of which means that a large fraction of the radar energy is reflected back to the radar. Dark features, indicating smooth surfaces (open water, flat sea-ice), yield no returns to the
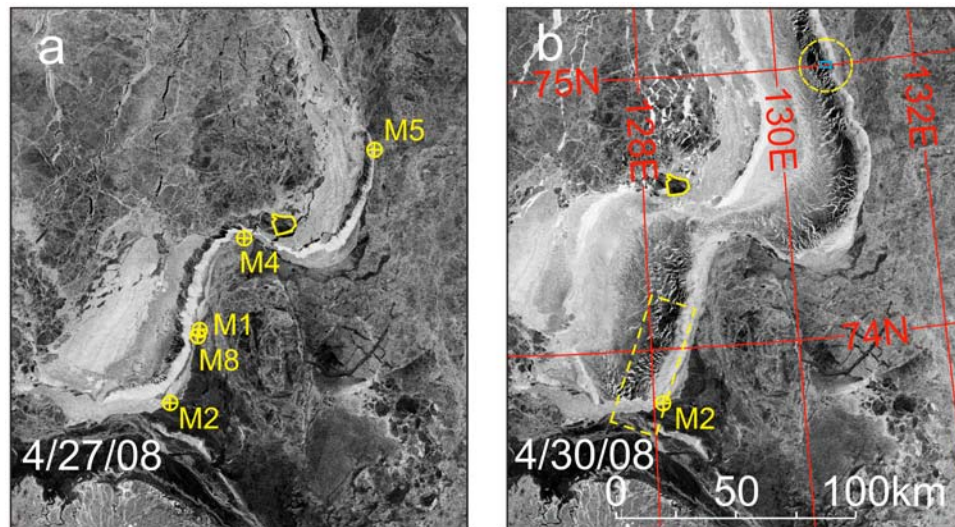
Figure 2. The sea-ice remote sensing observations of the coastal polynya event for 27–30 April 2008. The Envisat ASAR satellite imagery shows the evolution of the coastal polynya. (a) 27 April: circled yellow crosses indicate positions of oceanographic moorings equipped with SBE-37s and ADCPs. The yellow outline traces the broken fast-ice floe blown downwind from the fast-ice edge during polynya event. (b) 30 April: high radar backscatter strips appearing in gray/white indicate the frazil ice in the polynya area. Low radar backscatter features appearing in black indicate the open water. Yellow-dashed rectangle shows the spatial coverage of the TerraSAR-X high-resolution image shown in Figure 3a. Blue rectangle in the yellow-dashed circle at ~75°N indicates the location of polynya frazil ice strips as seen in the photo taken from the helicopter on 29 April (Figure 3c).

antenna. Radar backscatter from sea-ice depends on the dielectric properties and spatial distribution of the ice. Such factors as ice age, surface roughness, internal geometry, temperature, and snow cover will also all play a role in the affect of radar backscatter. For example, the new sea-ice in Figure 1, although a relatively flat surface, is much "rougher" than a calm water surface because of frost flowers that have been observed to grow on newly formed sea-ice from a saturated water vapor layer [*Style and Worster*, 2009].

[8] The Envisat ASAR images (Figures 1 and 2), obtained by using the C-band frequency, were acquired in a single vertical transmit and receive polarization configuration (VV) and in wide-swath mode. The images cover an area of approximately 400×800 km with a pixel spacing of 150 m and a spatial resolution of ~300 m. The TerraSAR-X imagery (Figures 3a and 3b) was obtained in strip-map mode and dual polarization (horizontal and vertical transmit and receive polarization: HH-VV), with a swath width of 15 km and a spatial resolution of 6.6 m in azimuth for the single-look complex data.

[9] The meteorological observations were carried out at four mooring positions (Figure 1) by using the automated weather stations (AWS). Data of air temperature, humidity, horizontal wind vector, net radiation, and barometric pressure were recorded with high temporal resolution. Polar bear attacks caused the loss of the M2 AWS data in the last 10 days of April. The nearest AWS at M1 located 33 km from M2 was recording only from 24 to 28 April (Figures 2 and 4). To fill this gap, we used Global Digital Analyses from the German Meteorological Service. To evaluate the global model GME [*Majewski et al.*, 2002], which has a horizontal resolution of 40 km, we used the AWS data. The

results show that the GME reasonably represents pressure and wind (correlation coefficients 0.8–0.9) and can be further utilized for our detailed polynya study.

3. Results

3.1. Sea-Ice and Meteorological Data

[10] The system of coastal polynyas over the southeastern Laptev Sea in April 2008 was not very well developed prior to the end of April, as exemplified by the Envisat ASAR image of 27 April (Figure 2a). The National Center for Environmental Prediction (NCEP), GME, and AWS surface wind data (Figure 4) indicate that three polynya favorable easterly southeasterly wind events were observed between 16 and 18 April (with winds up to 5–7 m/s), 22 and 23 April (up to 10 m/s), and 26 and 30 April (up to 12 m/s). The first wind event was not sufficient to create polynya; the second and mainly the third events, however, resulted in opening of a polynya. High-resolution simulations with the atmospheric model Consortium for Small-Scale Modeling (COSMO) (D. Schröder et al., Implementation of a thermodynamic sea-ice module in the NWP model COSMO and its impact on simulations for the Laptev Sea area in the Siberian Arctic, submitted to *Polar Research*, 2009) show that the total heat fluxes over the ice-free area varied between 600 and 900 W m^{-2} on 22–23 April and between 300 and 550 W m^{-2} on 26–30 April. The opening of frazil polynya (reaching up to 20 km in width) and columnar new-ice polynya (over a zone 40–50 km wide) are clearly evident in the satellite scenes from 30 April (Figure 2b) during a period of overall low air temperatures of about −12°C. Note that the terms frazil and columnar polynyas are used ac-
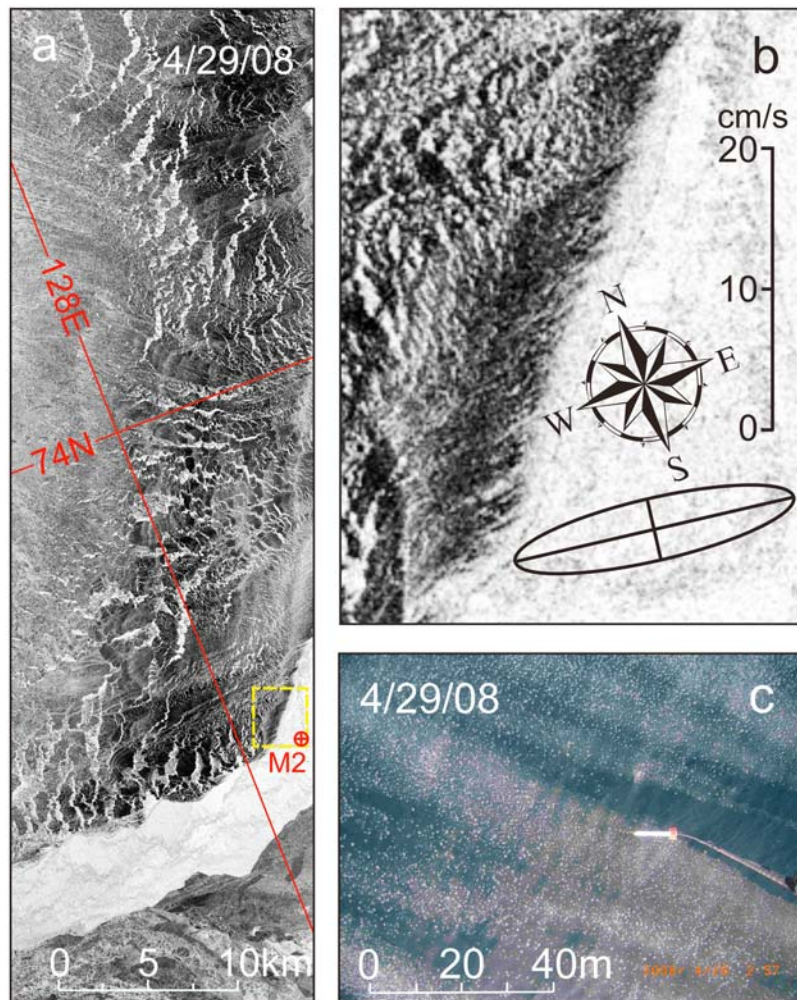
Figure 3. (a) TerraSAR-X high-resolution image (29 April 2008) of the fast-ice edge area shown in Figure 2b. Yellow-dashed rectangle contours the vicinity of M2 mooring enlarged in Figure 3b. (b) As in Figure 2b, high radar backscatter strips appearing in gray/white indicate the frazil ice; low radar backscatter features appearing in black indicate the open water. The tidal ellipse for the semidiurnal constituent M_2 (with scale indicated) was derived from the M2 ADCP velocity record between 5.4 and 7.4 m. (c) Aerial photo taken from the helicopter on 29 April at ~75°N (for location see Figure 2b) identifies polynya frazil ice strips. The dangling instrument is a helicopter-towed electromagnetic-induction system, a so-called EM bird, used for sounding sea-ice thickness (for more details see *Haas* et al. [2009]).

cording to *Danielson et al.* [2006] and *Drucker et al.* [2003]. For example, from 27 to 30 April, the broken fast ice floe was blown downwind from the vicinity of the fast ice edge by ~40 km (Figure 2). The TerraSAR-X scan from 29 April shows evidence of frazil ice formation occurring close to the fast ice edge and the columnar new-ice that occupies most of the polynya area (Figure 3a). The frazil ice polynya is also evident in the vicinity (in ~1 km) of the M2 mooring (Figure 3b) and farther north along the fast ice edge based on the TerraSAR-X scan (Figure 3a) and on the aerial photography (Figure 3c). Wind and waves set up a Longmuir circulation that forced the frazil ice into the long linear streaks. Later, winds decreased to 5–7 m/s and gradually aligned northeasterly, where they remained unchanged until the end of 3 May (Figure 4). On 1 May, the coastal polynya was almost fully covered with columnar new-ice (Figure 1) that, in fact, delineated the end-of-April frazil polynya event

(further denoted APE). Among all five moorings only M2 captured the APE because the other four moorings were recovered before 28 April.

3.2. Temperature, Salinity, and Velocity Data

[11] Figure 5 demonstrates a typical CTD profile taken at M2 on 24 April before the APE. The surface layer down to ~6 m at ~26.5 psu is likely dominated by under-ice tidal-driven mixing. The salinity difference between the surface and bottom layer (~4.5 psu) is due to the summer river runoff. The surface layer temperature is ~0.03°C above freezing.

[12] Figure 6a shows the time series of surface-layer residual currents at M2 obtained by a 25 h low-pass filtering of horizontal velocity components. In general, the under-ice flow is consistent with the mean wind-forcing, tending to flow ~5–35° to the right of the surface wind vector, except
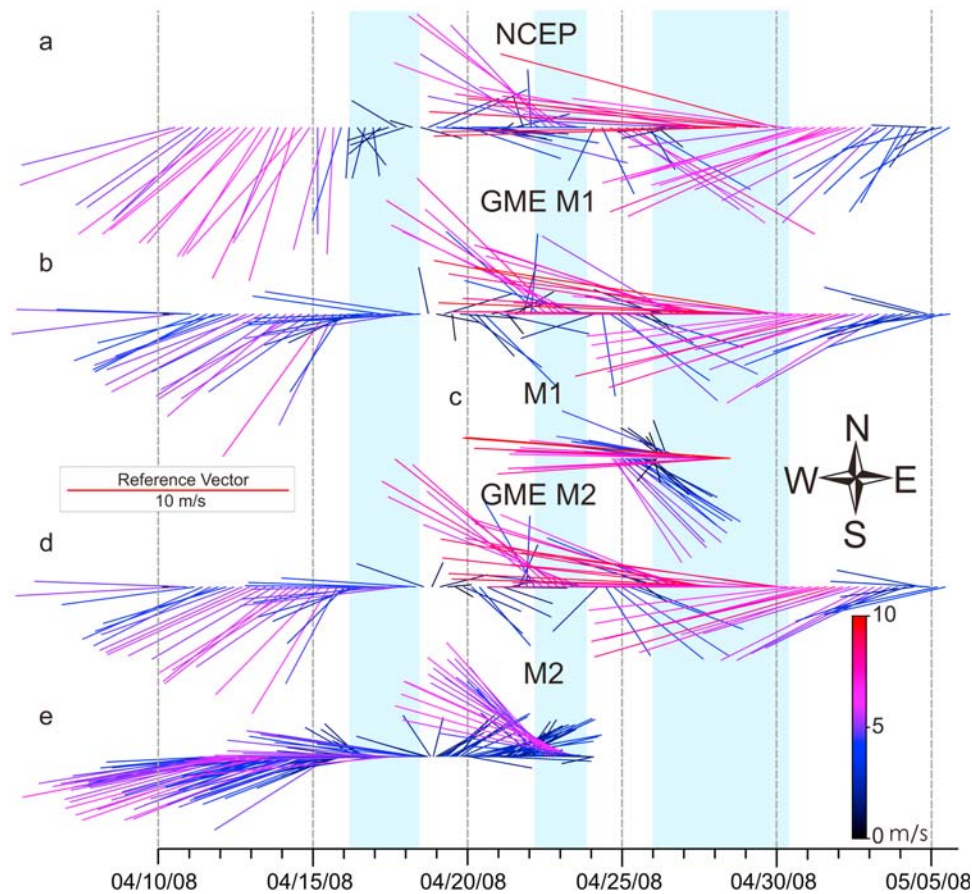
Figure 4. The stick plots of wind over the WNS coastal polynya. The length, color, and direction of each stick give the magnitude (m/s) and direction (°) of 2 h mean wind vector (true north is upward). (a) The National Center for Environmental Prediction (NCEP) wind at 75°N, 125.5°E, (b) global weather forecast model (GME) wind at M1, (c) AWS wind record at M1, (d) GME wind at M2, and (e) AWS wind record at M2. The periods of polynya favorable southeasterly wind are highlighted with blue shading.

for the weak wind-driven coupling during the second part of the APE (Figures 4 and 6a). Details of both the flow and salinity vary considerably, but two of the three salinity increase events (both by ~1.5 psu) on 12–13 April and 24–25 April involved a southwestward flow of ~5–7 cm/s. In contrast, the largest salinity increase, by ~4 psu, linked to the APE involved the northeastward flow of up to 18 cm/s (Figures 6a and 6b). Figure 6e shows the time series of the difference between the observed and the freezing temperature, where the freezing temperature was calculated by using a standard algorithm with the input of in situ depth and salinity by *Fofonoff and Millard* [1983]. Throughout the entire M2 record, only the sizable temperature drop to within ~0.02°C below freezing substantially exceeded the range of the SBE-37 temperature sensor accuracy of ±0.002°C (Figures 6e and 7). This supercooling event coincided with the APE.

[13] The velocity record is strongly influenced by tides (Figure 7). Amplitudes of the main tidal harmonics were estimated using an algorithm by *Foreman* [1977] and were averaged vertically through the surface layer down to the 7.4 m depth. For this layer, our tidal analysis revealed the predominance of lunar semidiurnal constituent M_2 (~70% of the tidal pattern) with an amplitude of 10.6 cm/s. The M_2

tidal ellipse had a clockwise rotation, the major axis being aligned to ~100° true (Figure 3b). Taking into account the mooring position relative to the fast ice edge and the M_2 tidal ellipse patterns (Figure 3), the tidal current would be sufficient to advect surface water from or to the polynya area by ~1.5–2 km in one tidal cycle. This is consistent with the recorded tidal semidiurnal oscillations in temperature and salinity with mean amplitudes of 0.01°C and 0.19 psu, respectively (Figures 6b, 6c, and 7). A maximum semidiurnal amplitude of ~0.04°C and ~1 psu was recorded from 30 April to 1 May at the very end of the APE. This large increase in the offshore salinity gradient characterizes the polynya salinity field with a strong salt source as a result of frazil ice formation during the polynya event. In fact, this tidal-forced thermohaline variability identifies a strong horizontal density gradient of ~1.62 kg/m³ created near the fast ice edge during the APE. The tidal southeastward currents from the polynya area caused an inflow of saltier and cooler water to the M2 site while the northwestward currents from beneath the fast ice supplied fresher and warmer water (not shown). Furthermore, during the APE the presence of relatively more supercooled water has been associated with tidal currents heading southeas (Figure 7).
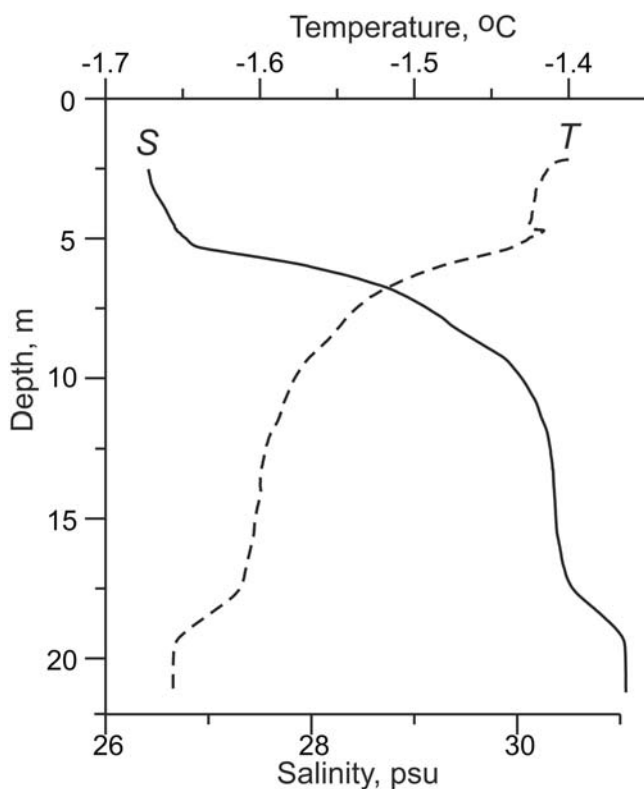
Figure 5. Vertical profiles of temperature (dashed line, °C) and salinity (solid line, psu) taken at M2 on 24 April before the end-of-April frazil polynya event (APE).

3.3. ADCP Acoustical Backscatter Data

[14] For the surface water layer down to 7.4 m, the ADCP acoustical backscatter (Figure 6d) negatively correlates with salinity (Figure 6b) and positively correlates with temperature (Figure 6c). Excluding the APE, we found statistically significant correlations (at the 95% confidence level) between the 1 h mean ADCP echo intensity measured at the 5.4 m bin and salinity and temperature of −0.49 and 0.43, respectively. This background pattern was disrupted during 28–29 April, when salinity and echo intensity increased simultaneously (Figures 6b and 6d). Throughout the entire period of the M2 observations, the APE in mean was the maximum scattering event observed by ADCP (Figure 6d). The recorded supercooling (Figure 6e) and the evidence of frazil ice seen on the TerraSAR-X imagery (Figures 3a and 3b) and on the aerial photographs (Figure 3c) for this period suggest that the scatterers are probably frazil ice crystals, even though we are not able to exclude air bubbles as potential scattering sources. Note, however, that the tidal-forced fraction of backscatter signal during the APE negatively correlates with salinity, so the individual high-scatter events in Figure 7 are not entirely associated with the occurrence of extreme supercooling.

4. Discussion

[15] Polynyas are characterized by high-salinity water at the freezing temperature. Once a water column is cooled to the freezing point, episodes of strong winds and low air temperature are expected to supercool water and generate frazil ice crystals, as reported in the Storfjorden polynya [*Skogseth et al.*, 2009]. The overwinter-moored upward looking sonar observations in the Bering Sea St. Lawrence Island polynya indicated higher surface layer acoustical scattering attributable to the frazil ice formation at polynya events [*Drucker et al.*, 2003]. The frazil ice crystals in the supercooled water plume have been inferred by echo sounding in the Prydz Bay, Antarctica [*Penrose et al.*, 1994]. Generally, ADCPs detect frazil ice in the water column [e.g., *Morse et al.*, 2006; *Richard and Morse*, 2008], but no absolute values of frazil ice concentration can be determined because a calibration is missing. Inspired by the theoretical analysis by *Jasek and Marko* [2007], our 307 kHz ADCP can detect particles having a diameter greater than ~1.5 mm that is, in general, consistent with the frazil ice particle diameter from 1–20 mm (for literature overview, see *Skogseth et al.* [2009]). For our maximum acoustical scattering event during the APE, the examination of the M2 data shows that the temperature fell to within 0.02°C below freezing, so that the remote sensing, wind, salinity, temperature, and acoustic observations appear to be consistent with polynya supercooled water and the presence of frazil ice crystals at the depths down to 7.4 m. This depth is also consistent with the surface layer depth (Figure 5).

[16] In the beginning of the APE, the surface layer exhibited mean northward flow from beneath the land-fast ice that is consistent with southeasterly winds (Figures 4 and 6a). The eastward tidal driven alignment of this flow results in polynya supercooled water observed at the mooring site (Figures 3b and 7). We also note that later the observed eastward aligned residual flow (Figure 6a) transported saltier and cooler water from the frazil polynya located to the west of M2 (Figures 3a, 6a, 6b, and 6c). We suggest that this flow was important in maintaining surface layer salinification by ~4 psu from 27 April to 2 May. This salinity range can be considered to be a measure of the salinity field adjustment to frazil polynya sea-ice formation. The relatively more supercooled water was associated with the semidiurnal tidal current aligning the mean flow in the direction from beneath the frazil polynya area. Afterward, the substantially weakened flow aligned to the southeast resulting in the gradual return to the pre-polynya thermohaline conditions (Figures 6a, 6b, and 6c).

[17] The overall impression from the M2 observations is that during most of the recorded period sizable temperature and salinity gradients were created across the fast ice edge by the surface wind forcing on the polynya and by the ocean response to this forcing (Figures 6b and 6c). A strong horizontal density gradient may give rise to geostrophic flow along the offshore edge of the polynya [*Danielson et al.*, 2006; *Gawarkiewicz and Chapman*, 1995; *Schumacher et al.*, 1983]. In contrast, the mean flow in the vicinity of the polynya appears to behave only modestly as predicted by geostrophic adjustment to the polynya-generated density field; most of the residual surface flow is controlled by the wind (Figures 4 and 6a). Only the northeastward motion over the M2 site during the last part of the APE would show a geostrophic tendency. This exception suggests that the local thermohaline patterns resulting from the strong
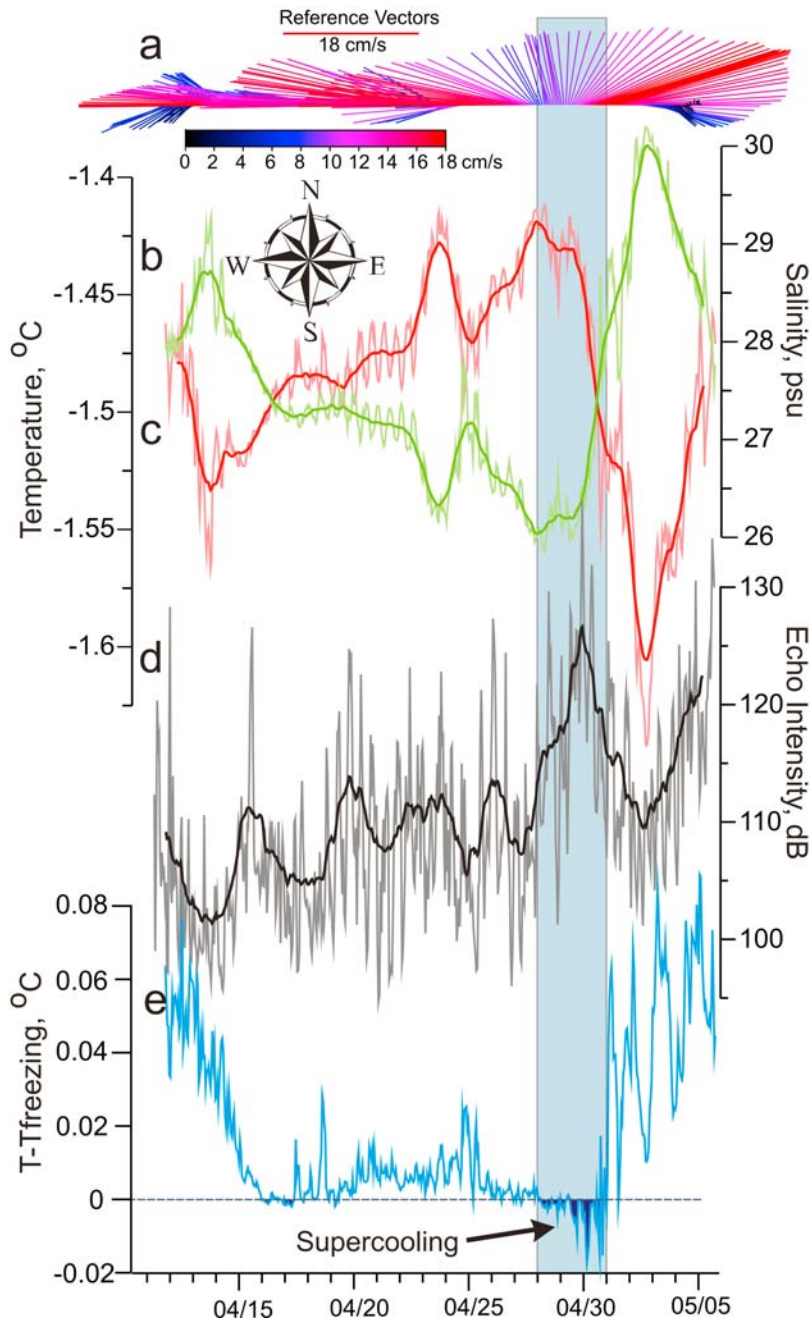
Figure 6. The M2 mooring time series from 11 April to 5 May 2008. (a) The stick plot of residual currents (1 h mean) from the upper ADCP bin measurements at 5.4 m. The length, color, and direction of each stick give the magnitude and direction of the current. The 1 h mean time series of (b) salinity (green, psu) and (c) temperature (red, °C) from 4.5 m, (d) echo intensity (black, dB) from 5.4 m, and (e) difference between the observed and the freezing temperature (blue, °C) from 4.5 m. The freezing temperature was calculated using a standard algorithm with the input of in situ depth and salinity by *Fofonoff and Millard* [1983]. The dark blue color marks supercooled conditions (also highlighted with blue shading). Bold lines show the 24 h running mean.

polynya events episodically can be more important in forcing the flow field than the regional wind.

5. Conclusions

[18] The paper examines under-ice-moored hydrographical and acoustic current data for April–May 2008 in the proximity of the fast ice edge of the West New Siberian coastal polynya, which is part of the Laptev Sea coastal polynya system. Combined with SAR satellite imagery, aerial photography, and meteorological data, the hydrographical response to the polynya activity has been studied with emphasis on the appearance of frazil ice seen both on
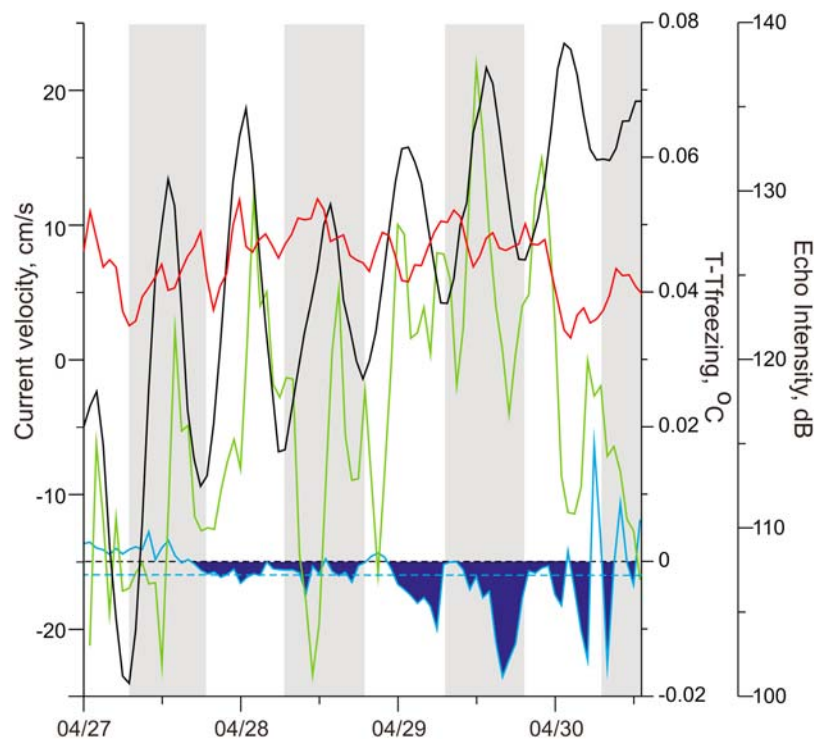
Figure 7. The enlarged portion of the 1 h mean M2 mooring record from the polynya event of 27–30 April 2008: (black) zonal and (red) meridional current velocity (cm/s) averaged vertically between 5.4 and 7.4 m; (green) echo intensity (dB) derived from the ADCP bin measurements at 5.4 m; (blue) difference between the observed and in situ freezing temperature from 4.5 m (°C). Dashed blue line shows the accuracy of the SBE-37 temperature sensor. Gray and white strips indicate lunar semidiurnal tidal cycle.

SAR satellite imagery and aerial photography, and through enhanced backscatter of the acoustic signals of ADCPs, when the polynya water is supercooled. Tides are dominated by the semidiurnal constituent and seem to have an effect on supercooling. We also find evidence for the persistent horizontal temperature and salinity gradients across the fast ice edge with the signature of geostrophic flow adjustment.

References

Bareiss, J., and K. Görgen (2005), Spatial and temporal variability of sea ice in the Laptev Sea: Analyses and review of satellite passive-microwave data and model results, 1979 to 2002, *Global Planet. Change*, *48*(1–3), 28–54, doi:10.1016/j.gloplacha.2004.12.004.

Coachman, L. K. (1966), Production of supercooled water during sea ice formation, in *Proceedings of the Symposium on Arctic Heat Budget and Atmospheric Circulation*, pp. 497–529, RAND Corp., Santa Monica, Calif.,

Danielson, S., K. Aagaard, T. Weingartner, S. Martin, P. Winsor, G. Gawarkiewicz, and D. Quadfasel (2006), The St. Lawrence polynya and the Bering shelf circulation: New observations and a model comparison, *J. Geophys. Res.*, *101*, C09023, doi:10.1029/2005JC003268.

Drucker, R., S. Martin, and R. Morits (2003), Observations of ice thickness and frazil ice in the St. Lawrence Island polynya from satellite imagery, upward looking sonar, and salinity/temperature moorings, *J. Geophys. Res.*, *108*(C5), 3149, doi:10.1029/2001JC001213.

Fofonoff, P., and R. C. Millard Jr. (1983), Algorithms for computation of fundamental properties of seawater, *UNESCO Tech. Pap. Mar. Sci.*, 44, 53 pp.

Foreman, M. G. G. (1977), Manual for tidal heights analysis and prediction, *Pac. Mar. Sci. Rep. 77–10*, 58 pp., Inst. of Ocean Sci., Patricia Bay, Sidney, B.C., Canada.

Gawarkiewicz, G., and D. C. Chapman (1995), A numerical study of dense water formation and transport on a shallow, sloping continental shelf, *J. Geophys. Res.*, *100*, 4489–4507, doi:10.1029/94JC01742.

Hass, C., J. Lobach, L. Rabenstein, and A. Pfaffling (2009), Helicopter-borne measurements of sea ice thickness, using a small and light-weight, digital EM system, *J. Appl. Geophys.*, *67*(3), 234–241, doi:10.1016/j.jappgeo.2008.05.005.

Jasek, M., and J. Marko (2007), Instrument for detecting suspended and surface ice runs in rivers, paper presented at the 14th Workshop on the Hydraulics of Ice Covered Rivers, Quebec City, Canada, Canad. Geophys. Union, Hydrol. Sect., Comm. on River Ice Processes and the Environment.

Majewski, D., D. Liermann, P. Prohl, B. Ritter, M. Buchhold, T. Hanisch, G. Paul, W. Wergen, and J. Baumgardner (2002), The operational global icosahedral-hexagonal grid point model GME: Description and high resolution tests, *Mon. Weather Rev.*, *130*, 319–338, doi:10.1175/1520-0493(2002)130<0319:TOGIHG>2.0.CO;2.

Martin, S., and D. J. Cavalieri (1989), Contributions of the Siberian Shelf polynyas to the Arctic Ocean intermediate and deep water, *J. Geophys. Res.*, *94*(C9), 12,725–12,738, doi:10.1029/JC094iC09p12725.

Morse, B., B. Ringo, D. Messier, T. Thanh-Quach, and E. Stander (2006), Hydrodynamics of mesotidal estuary in winter, *J. Cold Reg. Eng.*, *20*(3), 95–115, doi:10.1061/(ASCE)0887-381X(2006)20:3(95).

Penrose, J. D., M. Conde, and T. J. Pauly (1994), Acoustic detection of ice crystals in Antarctic waters, *J. Geophys. Res.*, *99*(C6), 12,573–12,580, doi:10.1029/93JC03507.

Richard, M., and B. Morse (2008), Multiple frazil ice blockages at a water intake in the St. Lawrence River, *J. Cold Reg. Eng.*, *53*, 131–149.

Schumacher, J. D., K. Aagaard, C. H. Pease, and R. B. Tripp (1983), Effects of a shelf polynya on flow and water properties in the northern Bering Sea (1983), *J. Geophys. Res.*, *88*(C5), 2723–2732, doi:10.1029/JC088iC05p02723.

Skogseth, R., L. H. Smedsrud, F. Nilsen, and I. Fer (2008), Observations of hydrography and downflow of brine-enrich shelf water in the Storfjord polynya, Svalbard, *J. Geophys. Res.*, *113*, C08049, doi:10.1029/2007JC004452.

Skogseth, R., F. Nilsen, and L. H. Smedsrud (2009), Supercooled water in an Arctic polynya: Observations and modeling, *J. Glaciol.*, *55*(189), 43–52, doi:10.3189/002214309788608840.

Style, R. W., and M. G. Worster (2009), Frost flower formation on sea ice and lake ice, *Geophys. Res. Lett.*, *36*, L11501, doi:10.1029/2009GL037304.

Zakharov, V. F. (1997), Sea ice in the climate system, *WMO/TD 782*, 80 pp., World Clim. Res. Prog. World Meteorol. Organ., Geneva, Switzerland.

T. Busche, German Aeropace Center, Microwaves and Radar Institute, PO Box 1116, D-82234 Wessling, Germany.

I. A. Dmitrenko, H. Kassens, T. Klagge, and C. Wegner, Leibniz Institute of Marine Sciences at University of Kiel (IFM-GEOMAR), Wischhofstr. 1-3, D-24148 Kiel, Germany. (idmitrenko@ifm-geomar.de)

G. Heinemann, A. Helbig, and D. Schröder, Department of Environmental Meteorology, University of Trier, Behringstr./Campus II, D-54286 Trier, Germany.

J. A. Hölemann and T. Krumpen, Alfred Wegener Institute for Polar and Marine Research, Am Handelshafen 12, D-27568 Bremerhaven, Germany.

S. A. Kirillov and K. P. Tyshko, Artic and Antarctic Research Institute, Bering St. 38, 199397 St. Petersburg, Russia.